Mechanistic Insights into the Pd-Catalyzed Carbonylation of Alkynol for α-Methylene-β-Lactone Formation

Xu Zhang[1,†], Wei Li[1,†], Tianqi Wang[1], Xurong Cao[1] and Lili Zhao[1,*]

[1]Informatization management center, State Key Laboratory of Materials-Oriented Chemical

Engineering, School of Chemistry and Molecular Engineering, Nanjing Tech University,

Nanjing 211816, China.

[*] Corresponding authors: ias_llzhao@njtech.edu.cn

[†]These authors contributed equally to this work.

Abstract: Density functional theory (DFT) calculations were performed to elucidate the reaction mechanism of the Pd-catalyzed carbonylation of propargylic alcohol **(1)**, leading to the efficient synthesis of cyclohexyl α-methylene-β-lactone **(2)**. Our study revealed that the reaction proceeds through a four-step pathway: alkyne migration and insertion, CO insertion, HCl-assisted hydrogen transfer, and final C–O annulation. Notably, the final C–O annulation step was identified as the rate-determining step (RDS) of the overall catalysis, with a free energy barrier of 25.7 kcal/mol (i.e., **IM4→TS4**). Additionally, we uncovered the critical role of the HCl during the reaction pathway, a demonstrating that it acts as a co-catalyst, proton shuttle, and hydrogen bond donor/acceptor. NBO, EDA-NOCV, and HIGM analyses further revealed that the remarkable stability of the transition state **TS3** in the presence of HCl primarily arises from strong electrostatic attraction and orbital interaction energies between the two interacting fragments. These mechanistic insights provide valuable insight and guidance for the rational design of new Pd-catalyzed transformations.
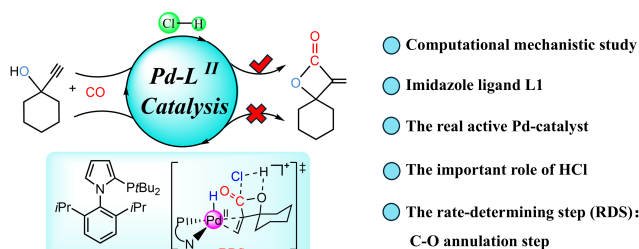
**Key words:** Reaction mechanism, α-Methylene-β-Lactones, Pd-catalyst, NBO analysis, EDA-NOCV analysis.

1. Introduction

α-Alkylidene-β-lactones are vital functional groups found in various biomolecules and pharmaceuticals, making them highly significant in medicinal chemistry [1,2].Their widespread occurrence in natural compounds and biologically active molecules has established them as key synthetic targets in organic synthesis [1-6], while their applications in materials science have also garnered considerable interest. Notably, α-methylene-β-lactones are particularly valuable due to their potential in ring-opening polymerization, enabling the synthesis

of copolymers with well-defined architectures, controlled molecular weights, and narrow polydispersity [7, 8] . In organic synthesis, the highly functionalized and compact structure of α-alkylidene-β-lactones provides diverse synthetic opportunities, making them versatile intermediates for further chemical transformations [9-15]. Additionally, their four-membered ring system is inherently strained, facilitating ring-opening reactions with various nucleophiles via acyl C-O or alkyl C-O bond cleavage [9, 16]. Given their synthetic importance, extensive efforts have been devoted to developing efficient methodologies for their preparation [17-22]. Reported strategies include [2+2]-cycloaddition of ketenes [23-26], lactonization of β-

hydroxycarboxylic acids and their derivatives [11, 17, 20, 21], selenoxide elimination from α-methyl-substituted lactones [27], and deoxygenation of β-peroxylactones [22, 28].

In 2020, Beller and co-workers reported the first general and highly selective Pd-catalyzed carbonylation of propargylic alcohols, leading to the efficient synthesis of α-methylene-β-lactones (i.e., **2**) [29]. This groundbreaking strategy highlights the pivotal role of Pd(II)-catalyst in achieving selective catalytic transformations. As shown in Scheme 1, the reaction proceeds under the catalytic influence of a phosphine palladium complex based on a 1-(2,6-diisopropylphenyl)-1H-imidazole ligand (**L-Pd**), where propargylic alcohol (**1**) undergoes carbonylation with CO, delivering the target product with high yield and excellent regioselectivity.
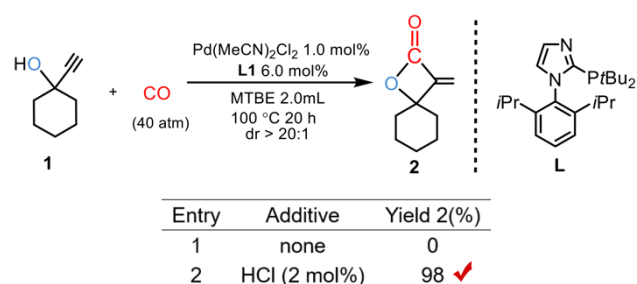
Scheme 1. Pd-catalyzed carbonylation of propargylic alcohols reported by Beller [29].

Although the authors proposed a plausible reaction pathway, several key aspects remain unresolved, including what the real active Pd-catalyst is, the role of HCl during the reaction pathway, and the identification of the rate-determining step (RDS) in the overall catalytic cycle. To bridge these gaps, we conducted a comprehensive density functional theory (DFT) study to elucidate the reaction mechanism of this transformation (Scheme 1). The mechanistic insight will not only enhance our understanding of the reaction but also provide a foundation for optimizing existing catalytic systems and guiding the development of new Pd-catalyzed strategies for α-alkylidene-β-lactone synthesis.

2. Theoretical method

Geometry optimizations were carried out with the Gaussian 16 program [30] and the structures were illustrated by CYLview [31]. Specifically, geometry optimizations without symmetry restriction were firstly optimized at the BP86 [32, 33]/def2-SVP [34, 35] level augmented with Grimme's D3 [36] dispersion corrections. Previous studies also calibrated the good performance of the BP86 functional for the Pd catalyzed reactions [37-39]. The solvation effects of the experimentally used solvent (i.e., toluene) were taken into consideration by using the integral equation formalism variant of polarizable continuum model IEFPCM [40]. Vibrational frequency calculations were performed at the same level of theory to characterize the stationary points as either local minima (no imaginary frequencies) or transition structures (one imaginary frequency) on the potential energy surface, and to obtain the thermochemical corrections for the Gibbs free energies. Intrinsic reaction coordinate (IRC)[41] calculations were conducted to verify the critical reaction steps involved in our proposed mechanisms. The energetic results were further improved by the single-point

calculations at the BP86-D3/def2-TZVPP [42] level with the solvation effects included. For comparison, the performance of several popular DFT functionals (e.g., B3LYP [43-45] , M06[46-48], B97D [49] and M06-L [50]) was studied on intermediate **IM4** (see Table S1), implying that the BP86 functional used in this study is reliable. Unless otherwise statement, the BP86-D3/def2-TZVPP (IEFPCM, solvent=toluene)//BP86-D3/def2-SVP (IEFPCM, solvent=toluene) Gibbs free energies (in kcal/mol) are used in the following discussion, while the electronic energies are also given in the related figures for reference. Spin natural orbital (SNO) analysis is given by Multiwfn 3.8 software [51]. NBO [52] calculations have been performed using NBO 3.1 program [53] implemented in the Gaussian 16 package at the same level of theory , The independent gradient model based on Hirshfeld partition (IGMH) [54] was employed to investigate the weak interactions of the transition state **TS3,TS3'** and **TS3''**, Using the AMS2024 program at the BP86/def2-SVP level,the nature of the bond in the transition state **TS3,TS3'** and **TS3''** was analyzed by combining the energy decomposition analysis (EDA) [55] with the natural orbital for chemical valence (NOCV) [56, 57].

3. Results and discussion

In this study, we first optimized two possible conformations of the cationic active palladium species. As shown in Scheme 2, **[L-Pd-H]**[+] is 2.5 kcal/mol more stable than its isomer **[H-L-Pd]**[+], implying that **[L-Pd-H]**[+] is the more favorable species and should be selected as the reference state for subsequent mechanistic investigations. The energetics results for the formation of the active **[L-Pd-H]**[+] species starting from the pre-catalyst Pd(MeCN)$_2$Cl$_2$ are provided in Figure S2. Notably, similar cationic active palladium species has been widely used in in previous studies [58, 59].
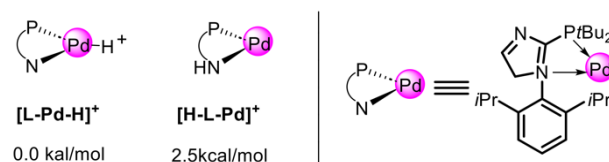
Scheme 2. Gibbs free energy difference for the **[L1-Pd-H]**[+] and **[H-L1-Pd]**[+] isomer.

Figure 1 presents the calculated free energy profiles for the formation of the α-methylene-β-lactone product (**2a**). Due to the coordination unsaturation of the cationic palladium hydride species [L-Pd-H][+], which renders it structurally unstable, this species readily coordinates with carbon monoxide (CO) to form a more stable intermediate [L-Pd(CO)H][+]. Subsequently, the CO ligand in [L-Pd(CO)H][+] is replaced via a ligand exchange process with the alkyne substrate (**1**), leading to the formation of the weakly coordinated palladium–alkyne complex **IM1**. In **IM1**, the H-atom in **[L-Pd-H]**[+] readily migrates to the terminal carbon of the alkyne (**1**) with a very low free energy barrier of 1.7 kcal/mol (i.e., **IM1→TS1**), yielding the slightly more stable intermediate **IM2**. In addition, we examined an alternative migratory insertion pathway involving a 1,2-insertion mode. However, the free energy barrier for the 1,2-insertion is 3.8 kcal/mol higher than that of the 2,1-insertion pathway (see Figure S3), implying that the 2,1-insertion pathway is kinetically more favorable, which agree well with experimentally observed selectivity.
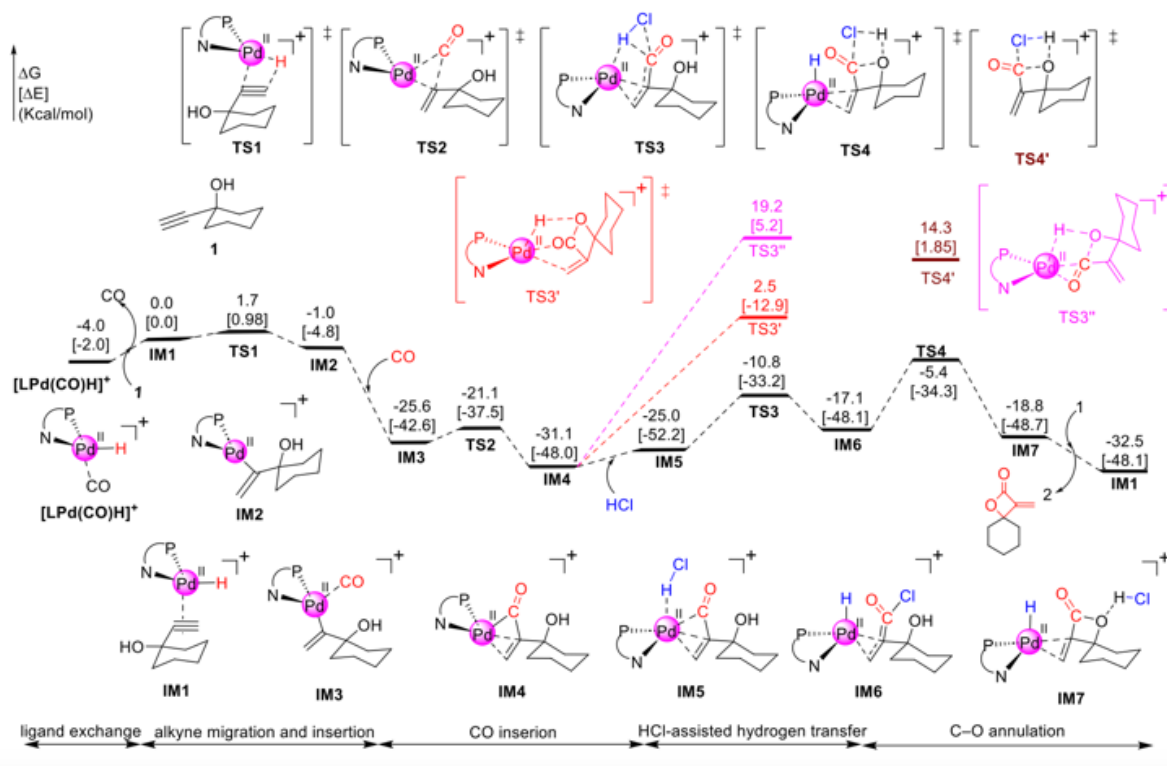
Figure 1. Computed Gibbs free energy profiles (in kcal/mol) for the target reaction.

Subsequent CO coordination leads to the thermodynamically more stable intermediate **IM3**, with an exergonic free energy release of 24.6 kcal/mol. After overcoming a small barrier of 4.5 kcal/mol via transition state **TS2**, the CO inserts into the Pd–C bond, yielding the more stable intermediate **IM4**.

The next step involves the addition of HCl, generating **IM5**, which is slightly less stable due to the inevitable entropy overestimated[60]. Upon crossing a barrier of 14.2 kcal/mol via transition state **TS3**, the proton from HCl is readily transferred to the Pd center, while Cl attaches to the carbonyl carbon, forming the acyl chloride intermediate **IM6**. The key bond distances in the optimized **TS3**, 1.588 Å, 1.758 Å, and 2.213 Å for the Pd—H, H—Cl and Cl—C bonds (see Figure 1), respectively, suggest the simultaneous formation of Pd–H and Cl–C bonds, along with H–Cl bond cleavage. The overall barrier, measured from the more stable **IM4**, is predicted to be 20.3 kcal/mol, which is experimentally accessible under mild conditions. The final C–O annulation occurs via transition state **TS4** with a free energy barrier of 11.7 kcal/mol (i.e., **IM6→TS4**), regenerating HCl for the next catalytic cycle. The key bond distances in **TS4** indicate that C–O cyclization and HCl liberation proceed in a concerted manner. With the addition of another equivalents of

reactant **1**, the final product **2** is liberated, and regenerating **IM1 f**or the next catalytic cycle. The final annulation step, with a free energy barrier of 25.7 kcal/mol, measured from the more stable intermediate **IM4**, is identified as the rate-determining step (RDS) during the entire catalytic cycle. The overall process is highly exergonic ($\Delta G =$ –32.5 kcal/mol), providing a strong thermodynamic driving force for the reaction to proceed efficiently.
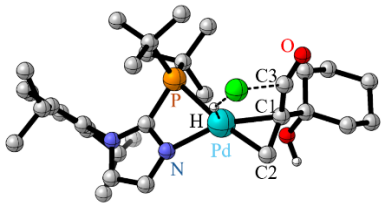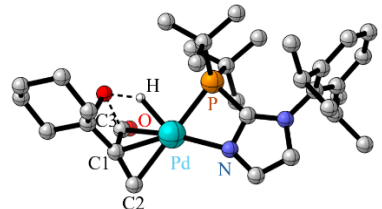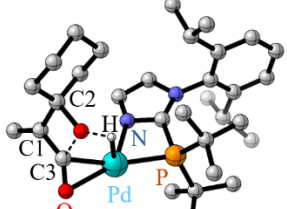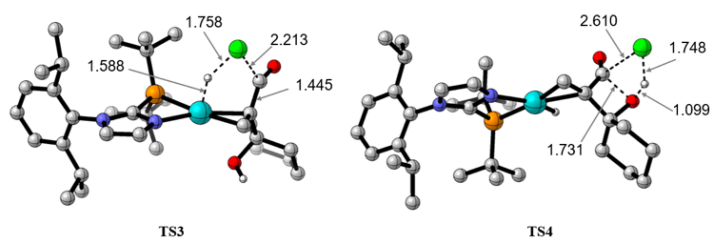

Figure 2. The optimized structures of the transition states **TS3** and **TS4.**

Table 1. The calculated NPA charge(q) f the optimized structures of **TS3**, **TS3'** and **TS3''** at the BP86/def-2TZVPP level.

	TS3		TS3'		TS3''

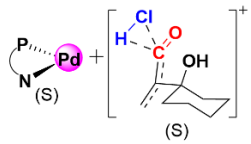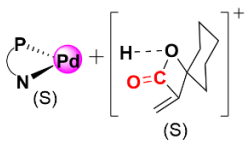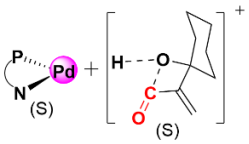| Species	NBO Analysis				
	Charges(q) derieved from Natural Population				
TS3	Pd	0.480	C1	-0.313	
	H	0.197	C2	-0.516	
	P	0.893	C3	0.677	
	N	-0.476	O	-0.377	
TS3'	Pd	0.321	C1	-0.205	
	H	0.272	C2	-0.498	
	P	1.012	C3	0.674	
	N	-0.487	O	-0.428	
TS3''	Pd	0.307	C1	-0.141	
	H	0.341	C2	-0.305	
	P	0.893	C3	0.539	
	N	-0.495	O	-0.45	

Additionally, we investigated alternative reaction pathways involving transition states **TS3'** and **TS3''**, where the annulation process proceeds without HCl. However, these pathways exhibit significantly higher free energy barriers of 33.6 kcal/mol (**IM4 → TS3'**) and 50.3 kcal/mol (**IM4 → TS3''**), respectively. These values are much greater than the 20.3 kcal/mol barrier observed for **TS3** (**IM4 → TS3**) and thus can be readily ruled out. This aligns well with experimental observations, where the reaction failed to proceed in the absence of HCl [29]. To address the role of HCl concentration, we performed additional calculations by introducing two and three HCl molecules into the **TS3** model. However, the introduce of multiple HCl molecules caused significant deviations from the original optimized reaction pathway, ultimately preventing the successful convergence of a corresponding transition states. It suggests that excess HCl disrupts the delicate balance of interactions at the active site, likely hindering rather than promoting the catalytic process. This outcome is consistent with experimental practice, where only a trace amount of HCl (2 mol%) is employed to achieve optimal reactivity without overwhelming the catalytic system.

To elucidate the critical role of HCl in stabilizing the key transition state **TS3** in the presence of HCl, we did Natural Bond Orbital (NBO) analysis. As detailed in Table 1, the Natural Population Analysis (NPA) charges on Pd in **TS3**, **TS3'**, and **TS3''** are 0.480, 0.321, and 0.307, respectively. These results suggest that the presence of HCl reduces the electron density around Pd in **TS3**,

enhancing its interaction with the substrate. The lower electron density also indicates a more uniform electron cloud distribution, which further contributes to stabilization. Consequently, the free energy barrier for **TS3** is significantly lower than those of **TS3'** and **TS3''**, underscoring the indispensable role of HCl in facilitating the reaction.

To further validate these findings, we performed Energy Decomposition Analysis coupled with Natural Orbital for Chemical Valence (EDA-NOCV) analysis to gain deeper insight into the critical role of HCl during the reaction pathway. As shown in Table 2, the transition state **TS3**, with HCl present, exhibits the lowest interaction energy (−172.6 kcal/mol) compared to **TS3'** and **TS3''**, explaining its enhanced stability. Specifically, although **TS3** has a relatively high Pauli repulsion energy (ΔE_{pauli} = 287.4 kcal/mol), this repulsion can be effectively compensated by the strong electrostatic attraction (ΔE_{elstat} = −221.5 kcal/mol) and orbital interaction energy (ΔE_{orb} = −222.9 kcal/mol), which is in good agreement with the larger NPA charge on Pd of **TS3** via NBO analysis. These two stabilizing factors, which contribute the 96.6% of the total attractive interactions, highlight the origin of **TS3**'s superior stability, reinforcing the crucial role of HCl in facilitating the annulation process. It is worthy of mentioning that the non-negligible dispersion forces in these three transition states are comparable (ca. 15 kcal/mol), which aligns with the Interaction Region Indicator (IRI) analysis (Figure 3). It means that the employment of the **L1** ligand

Table 2. EDA-NOCV results of [L1-Pd-sub] at the BP86/ def-2TZVPP level of theory. Fragments are given on table in singlet (S), Doublet(D) and Triplet(T) electronic states. Energy values are given in kcal/mol.

Species	TS3	TS3'	TS3''
Fragments			
ΔE_{int}	-172.6	-141.3	-101.6
ΔE_{Pauli}	287.4	226.1	129.4
ΔE_{elstat}	-221.5 (48.1%) [a]	-174.1 (47.4%)	-79.9 (34.6%)
ΔE_{disp}	-15.6 (3.4%) [a]	-14.5 (4.0%)	-15.6 (6.8%)
ΔE_{orb}	-222.9 (48.5%) [a]	-178.8 (48.7%)	-135.5 (58.7%)

[a]The values in parentheses give the percentage contribution to the total attractive interactions $\Delta E_{elstat} + \Delta E_{orb} + \Delta E_{disp}$.

also play important role in stabilizing the transitions state **TS3**, as shown by favorable C-H ---π, C-H---O interactions.

Figure 3. the Independent Gradient Model based on Hirshfeld Partition (HIGM) analysis of **TS3**,**TS3'** and **TS3''.**

4. Conclusion

In summary, DFT calculations were conducted to elucidate the reaction mechanism for the formation of cyclohexyl α-methylene-β-lactone (**2**) via the Pd-catalyzed carbonylation of alkynols **(1)**. Our study revealed that the overall catalytic cycle consists of four key steps: alkyne migration and insertion, CO insertion, HCl-assisted proton transfer, and final C–O annulation. Each step is both thermodynamically and kinetically feasible. Remarkably, the C–O annulation step, with a free energy barrier of 25.7 kcal/mol (i.e., **IM4→TS4**), was identified as the rate-determining step (RDS) of the entire catalytic cycle. Structural analysis of key transition states (**TS3, TS4**) and intermediates (**IM6, IM7**) demonstrated that HCl plays three critical roles: acting as a co-catalyst, proton shuttle, and hydrogen bond donor/acceptor. To gain deeper insight into the stabilizing effect of HCl on the key transition state **TS3**, we performed NBO, EDA-NOCV, and HIGM analyses. The results revealed that the strong electrostatic attraction (ΔE_{elstat} = −221.5 kcal/mol) and orbital interaction energy (ΔE_{orb} = −222.9 kcal/mol), are key factors contributing to the superior stability of **TS3**, reinforcing the crucial role of HCl in facilitating the annulation process. These mechanistic insights provide valuable guidance for
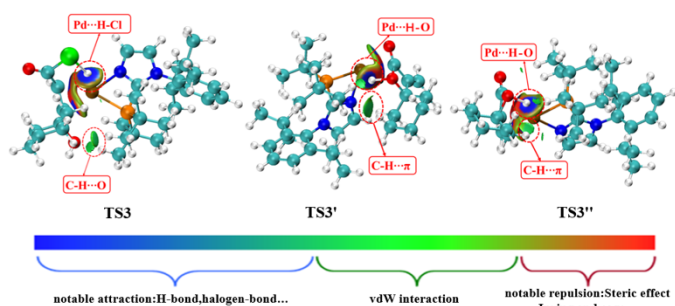
the rational design of new Pd-catalyzed transformations and the development of more efficient synthetic strategies.

Supporting information

Acknowledgements

References

[1] Kamat S. S., Camara K., Parsons W. H., Chen D.-H., Dix M. M., Bird T. D., Howell A. R., Cravatt B. F. Immunomodulatory lysophosphatidylserines are regulated by ABHD16A and ABHD12 interplay. *Nat. Chem. Bio.*, **11** (2) (2015), 164-171

[2] Parsons W. H., Kolar M. J., Kamat S. S., III A. B. C., Hulce J. J., Saez E., Kahn B. B., Saghatelian A., Cravatt B. F. AIG1 and ADTRP are atypical integral membrane hydrolases that degrade bioactive FAHFAs. *Nat. Chem. Bio.*, **12** (5) (2016), 367-372

[3] de Gutierrez A. N., Bardón A., Catalán C. A. N., Gedris T. B., Herz W. Sesquiterpene lactones and other constituents of *Disynaphia multicrenulata* from Argentina. *Bio. Sys. Eco.*, **29** (6) (2001), 633-647

[4] Bohlmann F., Paul A. H. K. Synthese einer modellverbindung für einen neuen guajanolid-typ. *Tetrahedron Lett.*, **25** (16) (1984), 1697-1700

[5] Bohlmann F., Zdero C., King R. M., Robinson H. 8β-Tigloylguaiagrazielolide from *Campovassouria bupleurifolia*. *Phytochem.*, **22** (12) (1983), 2860-2862

[6] Bohlmann F., Zdero C., King R. M., Robinson H. Germacranolides, a guaianolide with a β-lactone ring and further constituents from *Grazielia* species. *Phytochem.*, **20** (5) (1981), 1069-1075

[7] Hong M., Chen E. Y. X. Coordination ring-opening copolymerization of naturally renewable α-methylene-γ-butyrolactone into unsaturated polyesters. *Macromolecules*, **47** (11) (2014), 3614-3624

[8] Malapit C. A., Caldwell D. R., Sassu N., Milbin S., Howell A. R. Pd-catalyzed acyl C–O bond activation for selective ring-opening of α-methylene-β-lactones with amines. *Org. Lett.*, **19** (8) (2017), 1966-1969

[9] Yang C., Li B., Zhang X., Fan X. Synthesis of indenone-fused pyran derivatives from aryl enaminones and cyclopropenones through unsymmetrical relay C–H bond activation and double C–C/C–O bond formation. *Org. Lett.*, **26** (31) (2024), 6602-6607

[10] Wang Y., Huang Y., Bao X., Wei X., Wei S., Qu J., Wang B. Organocatalytic diastereo- and atropo-selective construction of eight-membered bridged (hetero)biaryls via asymmetric intramolecular [3 + 2] cycloaddition. *Chem. Sci.*, **15** (23) (2024), 8880-8887

[11] Sulwey D., DiSapio J. B., Gascón J. A., Howell A. R. 2-Halomethyleneoxetanes from 2-methyleneoxetanes by reaction with N-halosuccinimides: reactant influences on stereochemical outcomes and reaction pathways. *J. Org. Chem.*, **89** (22) (2024), 16571-16585

[12] Fan T., Shi Z., Gong Q.-W., Song J., Gong L.-Z. Rhodium and isothiourea dual catalysis: enantiodivergent transformation of terminal alkynes. *Org. Lett.*, **26** (7) (2024), 1421-1425

[13] Zhu G., Shi W., Gao H., Zhou Z., Song H., Yi W. Chemodivergent couplings of N-arylureas and methyleneoxetanones via Rh(III)-catalyzed and solvent-controlled C–H activation. *Org. Lett.*, **21** (11) (2019), 4143-4147

[14] Danheiser R. L., Choi Y. M., Menichincheri M., Stoner E. J. Synthesis of allenes via thermal cycloreversion of α-alkylidene-β-lactones. *J. Org. Chem.*, **58** (2) (1993), 322-327

[15] Adam W., Salgado V. O. N., Peters E.-M., Peters K., Schnering H. G. V. Stereoselective synthesis of α,β-trans-spiro-β-lactones by Diels–Alder cycloaddition of 1,3-dienes to α-methylene-β-lactone and their decarboxylation by pyrolysis to (E)-alkylidenecycloalkenes, a convenient olefination method. *Chem. Ber.*, **126** (6) (1993), 1481-1486

[16] Adam W., Hasemann L. α-Methylene β-S-thiolactones: synthesis of a new heterocycle by sulfurization of an α-methylene β-lactone and its structure. *Chem. Ber.*, **123** (6) (1990), 1449-1451

[17] Zhang C. M., Lu X. Y. Stereoselective synthesis of methyl (Z)-3-iodo-2-(1-hydroxyalkyl)prop-2-enoates and their further transformation to α-(Z)-iodomethylene-β-lactones. *Synthesis-Stuttgart*, (5) (1996), 586-&

[18] Adam W., Hasemann L., Prechtl F. α-Methylen-β-lacton, ein neuer Heterocyclus durch Desoxygenierung von α-Methylen-β-peroxylactonen mit Triphenylphosphan. *Angew. Chem.*, **100** (11) (1988), 1594-1595

[19] Adam W., Hasemann L., Prechtl F. α-Methylene-β-lactone, a novel heterocyclic ring system via deoxygenation of α-methylene-β-peroxylactones with triphenylphosphane. *Angew. Chem. Int. Ed.*, **27** (11) (1988), 1536-1537

[20] Roso-Levi G., Amer I. Synthesis of α-methylene-β-lactones by nickel-catalyzed hydrocarboxylation of propargyl alcohols. *J. Mol. Cat. A*, **106** (1-2) (1996), 51-56

[21] Bartels A., Jones P. G., Liebscher J. Stereoselective diazoalkane cycloadditions to chiral 5-alkylidene-1,3-dioxan-4-ones and 3-benzylidene-β-lactones. *Synthesis-Stuttgart*, (11) (1998), 1645-1654

[22] Adam W., Albert R., Dachs Grau N., Hasemann L., Nestler B., Peters E. M., Peters K., Prechtl F., von Schnering H. G. Synthesis of α-methylene β-lactones, novel heterocycles. *J. Org. Chem.*, **56** (20) (1991), 5778-5781

[23] Adam W., Salgado V. O. N., Peters E.-M., Peters K., Schnering H. G. V. Stereoselective synthesis of α,β-trans-spiro-β-lactones by Diels–Alder cycloaddition of 1,3-dienes to α-methylene-β-lactone and their decarboxylation by pyrolysis to (E)-alkylidenecycloalkenes, a convenient olefination method. *Chem. Ber.*, **126** (6) (1993), 1481-1486

[24] Payne G. B. Reactions of α,β-unsaturated acid chlorides with tertiary amines. *J. Org. Chem.*, **31** (3) (1966), 718-721

[25] Baxter G., Brown R., Eastwood F., Gatehouse B., Nesbit M. Methyleneketenes and methylenecarbenes. XIII. Cycloaddition of ketenes and of a 1-pyrroline 1-oxide to isopropylideneketene. *Aust. J. Chem.*, **31** (8) (1978), 1757-1767

[26] Masters A., Sorensen T. Low temperature ketene preparations using nitrosyltetracarbonylchromium(−II) anion. *Tetrahedron Lett.*, **30** (43) (1989), 5869-5872

[27] Danheiser R. L., Choi Y. M., Menichincheri M., Stoner E. J. Synthesis of allenes via thermal cycloreversion of α-alkylidene-β-lactones. *J. Org. Chem.*, **58** (2) (1993), 322-327

[28] Adam W., Hasemann L. α-Methylene β-S-thiolactones: synthesis of a new heterocycle by sulfurization of an α-methylene β-lactone and its structure. *Chem. Ber.*, **123** (6) (1990), 1449-1451

[29] Ge Y., Ye F., Liu J., Yang J., Spannenberg A., Jiao H., Jackstell R., Beller M. Ligand-controlled palladium-catalyzed carbonylation of alkynols: highly selective synthesis of α-methylene-β-lactones. *Angew. Chem. Int. Ed.*, **59** (48) (2020), 21585-21590

[30] Frisch M. J., Trucks G. W., Schlegel H. B., Scuseria G. E., Robb M. A., Cheeseman J. R., et al. *Gaussian 16 Rev. A.03*, Gaussian Inc., Wallingford CT (2016)

[31] Legault C. Y. *CYLview 1.0b*, Université de Sherbrooke (2009)

[32] Perdew J. P. Density-functional approximation for the correlation energy of the inhomogeneous electron gas. *Phys. Rev. B*, **33** (12) (1986), 8822-8824

[33] Lee C., Yang W., Parr R. G. Development of the Colle-Salvetti correlation-energy formula into a functional of the electron density. *Phys. Rev. B*, **37** (2) (1988), 785-789

[34] Zhao Y., Truhlar D. G. The M06 suite of density functionals for main-group thermochemistry, thermochemical kinetics, noncovalent interactions, excited states, and transition elements: two new functionals and systematic testing of four M06-class functionals and 12 other functionals. *Theor. Chem. Acc.*, **120** (1-3) (2008), 215-241

[35] Weigend F. Accurate Coulomb-fitting basis sets for H to Rn. *PCCP*, **8** (9) (2006), 1057-1065

[36] Grimme S., Antony J., Ehrlich S., Krieg H. A consistent and accurate *ab initio* parametrization of density functional dispersion correction (DFT-D) for the 94 elements H-Pu. *J. Chem. Phys.*, **132** (15) (2010)

[37] Liu W., Liu Z., Liu X., Dang Y. Mechanism of Pd-catalysed C(sp3)–H arylation of thioethers with Ag(I) additives. *Org. Bio. Chem.*, **19** (31) (2021), 6766-6770

[38] Ke Z., Cundari T. R. Palladium-catalyzed C–H activation/ C–N bond formation reactions: DFT study of reaction mechanisms and reactive intermediates. *Organometallics*, **29** (4) (2010), 821-834

[39] Zhao X., Zhang D., Wang X. Unraveling the mechanism of palladium-catalyzed base-free cross-coupling of vinyl carboxylates: dual role of arylboronic acids as a reducing agent and a coupling partner. *ACS Catal.*, **12** (3) (2022), 1809-1817

[40] Miertuš S., Scrocco E., Tomasi J. Electrostatic interaction of a solute with a continuum: a direct utilization of *ab initio* molecular potentials for the prevision of solvent effects. *Chem. Phys.*, **55** (1) (1981), 117-129

[41] Fukui K. The path of chemical reactions – the IRC approach. *Acc. Chem. Res.*, **14** (12) (1981), 363-368

[42] Weigend F., Ahlrichs R. Balanced basis sets of split valence, triple zeta valence and quadruple zeta valence quality for H to Rn: design and assessment of accuracy. *PCCP*, **7** (18) (2005), 3297-3305

[43] Grimme S., Ehrlich S., Goerigk L. Effect of the damping function in dispersion-corrected density functional theory. *J. Comput. Chem.*, **32** (7) (2011), 1456-1465

[44] Grimme S., Antony J., Ehrlich S., Krieg H. A consistent and accurate *ab initio* parametrization of density functional dispersion correction (DFT-D) for the 94 elements H-Pu. *J. Chem. Phys.*, **132** (15) (2010)

[45] Becke A. D. Density-functional thermochemistry. III. The role of exact exchange. *J. Chem. Phys.*, **98** (7) (1993), 5648-5652

[46] Li Y., Chen H., Qu L.-B., Houk K. N., Lan Y. Origin of regiochemical control in Rh(III)/Rh(V)-catalyzed reactions of unsaturated oximes and alkenes to form pyridines. *ACS Catal.*, **9** (8) (2019), 7154-7165

[47] Chen H., Zhu L., Zhong K., Yue X., Qu L.-B., Bai R., Lan Y. Theoretical insight into phosphoric acid-catalyzed asymmetric conjugate addition of indolizines to α,β-unsaturated ketones. *Chin. Chem. Lett.*, **29** (8) (2018), 1237-1241

[48] Zhao Y., Truhlar D. G. Density functionals with broad applicability in chemistry. *Acc. Chem. Res.*, **41** (2) (2008), 157-167

[49] Grimme S. Semiempirical GGA-type density functional constructed with a long-range dispersion correction. *J. Comput. Chem.*, **27** (15) (2006), 1787-1799

[50] Zhao Y., Truhlar D. G. A new local density functional for main-group thermochemistry, transition metal bonding, thermochemical kinetics, and noncovalent interactions. *J. Chem. Phys.*, **125** (19) (2006)

[51] Lu T., Chen F. Multiwfn: a multifunctional wavefunction analyzer. *J. Comput. Chem.*, **33** (5) (2012), 580-592

[52] Reed A. E., Curtiss L. A., Weinhold F. Intermolecular interactions from a natural bond orbital, donor-acceptor viewpoint. *Chem. Rev.*, **88** (6) (1988), 899-926

[53] Glendening E. D., Baden J. K., Reed A. E., Carpenter J. E., Weinhold F. *NBO Version 3.1*, Theoretical Chemistry Institute, University of Wisconsin, Madison

[54] Lu T., Chen Q. Independent gradient model based on Hirshfeld partition: a new method for visual study of interactions in chemical systems. *J. Comput. Chem.*, **43** (8) (2022), 539-555

[55] Ziegler T., Rauk A. On the calculation of bonding energies by the Hartree–Fock–Slater method. *Theor. Chim. Acta*, **46** (1) (1977), 1-10

[56] Mitoraj M., Michalak A. Donor–acceptor properties of ligands from the natural orbitals for chemical valence. *Organometallics*, **26** (26) (2007), 6576-6580

[57] Mitoraj M., Michalak A. Applications of natural orbitals for chemical valence in a description of bonding in conjugated molecules. *J. Mol. Model.*, **14** (8) (2008), 681-687

[58] Gies A. P., Zhou Z., Mukhopadhyay S., Kosanovich A. J., Keaton R. J., Auyeung E., Kobylianskii I., Beezer D. B., Dau H., Harth E. Analytical insights into the microstructures and reaction mechanisms of cationic Pd(II) α-diimine-catalyzed polyolefins. *Macromolecules*, **54** (23) (2021), 10814-10829

[59] Shen K., Han X., Lu X., Hu Z. Cationic Pd(II)-catalyzed arylative cyclization of 1,6-enynes with arylboronic acids. *Tetrahedron Lett.*, **58** (39) (2017), 3768-3771

[60] Ben-Naim A., Marcus Y. Solvation thermodynamics of nonionic solutes. *J. Chem. Phys.*, **81** (4) (1984), 2016-2027